The 1995 pilot campaign of PLANET: searching for microlensing anomalies through precise, rapid, round-the-clock monitoring

Albrow, M.; Beaulieu, J.P.; Birch, P.; Caldwell, J.A.R.; Kane, S.; Martin, R.; Menzies, J.; Naber, R.; Pel, J.W.; Pollard, K.; Sackett, P.D.; Sahu, K.C.; Vreeswijk, P.M.; Williams, A.; Zwaan, M.A.

DOI
10.1086/306513

Publication date
1998

Published in
Astrophysical Journal

THE ASTROPHYSICAL JOURNAL, 509:687–702, 1998 December 20

THE 1995 PILOT CAMPAIGN OF PLANET: SEARCHING FOR MICROLENSING ANOMALIES THROUGH PRECISE, RAPID, ROUND-THE-CLOCK MONITORING

M. ALBROW,[1,2] J.-P. BEAULIEU,[3] P. BIRCH,[4] J. A. R. CALDWELL,[1] S. KANE,[5,6] R. MARTIN,[4] J. MENZIES,[1] R. M. NABER,[3] J.-W. PEL,[3] K. POLLARD,[1] P. D. SACKETT,[3] K. C. SAHU,[6] P. VREESWIJK,[3] A. WILLIAMS,[4] AND M. A. ZWAAN[3]
(THE PLANET COLLABORATION)
Received 1998 January 14; accepted 1998 July 27

ABSTRACT

PLANET (the Probing Lensing Anomalies NETwork) is a worldwide collaboration of astronomers whose primary goal is to monitor microlensing events densely and precisely in order to detect and study anomalies that contain information about Galactic lenses and sources that would otherwise be unobtainable. The results of PLANET's highly successful first year of operation are presented here. Details of the observational setup, observing procedures, and data-reduction procedures used to track the progress in real time at the three participating observing sites in 1995 are discussed. The ability to follow several events simultaneously with a median sampling interval of 1.6 hr and a photometric precision of better than 0.10 mag even at $I = 19$ has been clearly demonstrated. During PLANET's 1995 pilot campaign, ten microlensing events were monitored, resulting in the most precise and densely-sampled light curves to date; the binary nature of one of these, MACHO 95-BLG-12, was recognized by PLANET on the mountain. Another event, OGLE 95-BLG-04, displayed chromaticity that may betray the presence of blending with unresolved stars projected onto the same resolution element. Although lasting only about a month, the campaign may allow constraints to be placed on the number of planets with mass ratios to the parent star of 0.01 or greater.

Subject headings: Galaxy: stellar content — gravitational lensing — planetary systems — stars: variables: other — surveys

1. INTRODUCTION

The phenomenon of gravitational microlensing, the apparent brightening and subsequent dimming of a background star as the gravitational field of a moving foreground star or other object alters the light path of the background source, was predicted by Einstein in 1936 (Einstein 1936). Because of the precise alignment required for a detectable brightening, the chance of a substantial microlensing magnification is extremely small (on the order of 1×10^{-6}) for background stars in the Galactic bulge or nearby Magellanic Clouds, even if all the unseen Galactic dark matter is composed of objects capable of lensing (Paczyński 1986). For this reason, it was not until 1993, when massive observational programs capable of surveying millions of stars were well underway, that microlensing was observed toward the Galactic bulge and Magellanic Clouds by the EROS, MACHO, and OGLE projects (Aubourg et al. 1993, Alcock et al. 1993, Udalski et al. 1993). Gravitational microlensing toward the Galactic bulge and the Large Magellanic Cloud (LMC) has now been convincingly demonstrated by the more than 200 microlensing events detected by these microlensing survey teams. Other groups have joined the hunt by adding more events in the bulge (Alard & Guibert 1997) and candidate events in the nearby spiral M31 (Crotts & Tomaney 1996), while still others are just beginning to collect data in the LMC (Abe et al. 1997) and M31 (Melchior 1997). Microlensing is providing new information on the amount of mass (dark and luminous) along these lines of sight (Paczyński 1996), although the nature of the unseen lenses is still a matter of considerable debate and accurate interpretation will require more data (Mao & Paczyński 1996). Reviews on the subject of microlensing can be found in Paczyński (1996) and Gould (1996).

The field of microlensing has quickly matured to the point that events are now reliably detected and reported while they are still in progress; the OGLE and MACHO teams have issued over 150 real-time electronic "alerts," nearly all in the direction of the Galactic bulge (Pratt et al. 1996, Udalski et al. 1994a). This capability has stimulated the birth of second-generation projects such as PLANET (Albrow et al. 1996; Albrow et al. 1997) and GMAN (Pratt et al. 1996) that gather detailed photometric information about individual events, producing a refined understanding of the primary light curve. Other groups dedicated to obtaining high-quality spectroscopy of microlensing events are also in place (Lennon et al. 1996). Most importantly, microlensing monitoring data of sufficient precision and quantity allows the detection and characterization of microlensing *anomalies*, fine structure in the light curves that contain detailed information about the nature of source and lens populations. As a result, new fields of study are just beginning to open up as microlensing monitoring gives astronomy a tool with which to study the kinematics of lenses, the stellar mass function, the frequency and nature of binary systems, stellar atmospheres, and to use in the detection and characterization of brown dwarfs and extrasolar planets.

Galactic microlensing survey experiments are optimized

[1] South African Astronomical Observatory, P.O. Box 9, Observatory 7935, South Africa.
[2] University of Canterbury, Department of Physics and Astronomy, Private Bag 4800, Christchurch, New Zealand.
[3] Kapteyn Astronomical Institute, Postbus 800, 9700 AV Groningen, The Netherlands.
[4] Perth Observatory, Walnut Road, Bickley, Perth 6076, Australia.
[5] University of Tasmania, Physics Department, G.P.O. 252C, Hobart, Tasmania 7001, Australia.
[6] Space Telescope Science Institute, 3700 San Martin Drive, Baltimore, MD 21218.

to maximize the detection rate of microlensing events, but they are ill suited to the detection and characterization of most anomalies, necessitating a separate monitoring effort. The PLANET (Probing Lensing Anomalies NETwork) collaboration uses a worldwide network of telescopes to obtain the frequent, precise observations required for a study of these anomalies. In particular, PLANET observations are optimized for the detection of anomalies caused by planets orbiting distant Galactic lenses, a subject that has come to the fore of scientific and public attention recently, with the apparent detection via other techniques of nearby extrasolar planets. Described here are the results of the PLANET 1995 pilot campaign, during which ten microlensing events were observed for approximately 4 weeks from three semidedicated locations in the southern hemisphere. This campaign resulted in the most precise and densely sampled microlensing light curves to date and the real-time detection of one binary system.

A summary of microlensing anomalies and the information that they contain is given in § 2. The PLANET collaboration is discussed in § 3, and the details of its 1995 pilot season are given in § 4. A description of the data-reduction procedures appears in § 5, and a discussion of the photometric errors follows in § 6. The resulting microlensing light curves are presented and discussed in § 7. Conclusions and final remarks can be found in § 8.

2. MICROLENSING ANOMALIES

The ability of the survey teams to find microlensing needles in the dense stellar haystacks of the Galactic bulge and LMC has relied most heavily on the simple, symmetric, achromatic, and nonrepeating light curve that distinguishes simple microlensing from other variable phenomena. The form of this light curve, which is appropriate to lensing geometries in which both the point-source and point-lens approximations are valid and all motions are rectilinear, can be characterized by four parameters: the maximum magnification $A_{\max}$, the time of maximum magnification t_0, the baseline flux F_0, and a characteristic width of the light curve, t_E.

The angular "range of influence" of a point lens is characterized by its Einstein ring radius θ_E, which is a function of the lens mass M and the lens-source geometry:

$$\theta_E = \sqrt{\frac{4GMD_{LS}}{c^2 D_L D_S}}\,, \tag{1}$$

where D_S is the observer-source distance, D_L the observer-lens distance, and D_{LS} the source-lens distance. Galactic microlensing by stars or other objects of similar mass generates two images separated by a distance equal to or greater than $2\theta_E$, which for typical geometries and masses is on the order of 1 mas, and thus too small to be resolved by conventional techniques.

The combined time-variable flux $F(t)$ of the two microimages, on the other hand, is detectable, and is given by

$$F(t) = A(t)F_0\,, \tag{2}$$

where F_0 is the unlensed (baseline) source flux and $A(t)$ is the changing microlensing magnification due to the relative motions of the observer, lens, and source. For a point source separated by an angular distance θ_{LS} at time t from a point lens, the magnification $A(t)$ is a simple function of the normalized angular separation $u(t) \equiv \theta_{LS}/\theta_E$:

$$A(t) = \frac{u^2(t) + 2}{u(t)\sqrt{u^2(t) + 4}}\,. \tag{3}$$

Rectilinear motion of the observer-lens-source geometry in which the lens moves with speed $v_\perp$ across the observer-lens line of sight results in a time dependence for $u(t)$ given by

$$u(t) = \sqrt{\frac{(t - t_0)^2}{t_E} + u_{\min}^2}\,, \tag{4}$$

where t_0 is the time at peak magnification [when $u(t)$ attains its minimum value $u_{\min}$] and $t_E \equiv D_L\theta_E/v_\perp$ is the time required for the source to cross an Einstein ring radius.

For a given population of lenses, reasonable estimates can be made for the amplitude and duration of microlensing light curves. Sources lying inside the Einstein ring in projection (i.e., with $\theta_{LS} < \theta_E$ and thus $u_{\min} < 1$) will have peak magnifications A in excess of 1.34. Statistically, the peak magnifications will be distributed linearly in $u_{\min}$, with smaller $u_{\min}$ resulting in higher magnification A, approaching $A = 1/u_{\min}$ as $u_{\min} \to 0$. A source in the Galactic bulge moving with a speed of 200 km s^{-1} with respect to a 1 $M_\odot$ lens located halfway between the source and the observer will have an Einstein time t_E of $\sim$35 days. Because of the form of the stellar initial mass function and the distribution of Galactic light, typical stellar lenses are probably less massive and located closer to the Galactic center, resulting in a somewhat smaller typical t_E. The length of time that a typical Galactic event is above the canonical $A = 1.34$ would be expected to be less than $2t_E$, and thus on the order of weeks to months, roughly matching the observed value (Alcock et al. 1997a).

Microlensing anomalies are departures from the achromatic light curve given by equations (2)–(4). Such departures are expected in the case of multiple lenses, multiple point sources or blends along the line of sight, extended sources, and complicated relative motion within the source-lens–observer system. Thus, anomalies, if well characterized, can be used to extract detailed information about source and lens populations. Such information is sorely needed for the interpretation of the primary survey data, since of the four standard microlensing parameters, three contain no information about the lens, and the fourth, the characteristic Einstein time t_E, is a degenerate combination of the lens mass, distance, and relative velocity. Examples of microlensing anomalies and the extra science that they can provide are detailed below.

2.1. *Lensing Binary Systems*

Multiple lenses separated by a distance of up to a few Einstein ring radii do not behave like isolated lenses. The axial symmetry of the magnification pattern is destroyed, and nonlinear effects generate caustic structure projected onto the source plane. Sources crossing caustic curves will exhibit sharp enhancements in their light curves, with durations of a few hours, while inside the curve the magnification will remain elevated as a result of the generation of additional images. The magnification pattern outside the caustic curve is also distorted relative to that in the single point-lens case; thus, detectable light curve anomalies with a wealth of morphologies can be generated by multiple lens systems even if no caustic crossings occur. The OGLE

group made the first clear detection of a binary lens in 1993 (Udalski et al. 1994b), and since then several more have been reported (Alard, Mao, & Guibert 1995; Alcock et al. 1997a). Modeling of the well-sampled binary light curves yields the binary mass ratio and the binary separation in units of θ_E. Such events thus contain information about lensing binaries too faint to be detected by other methods in the disk and bulge of the Galaxy (Dominik & Hirshfeld 1994; Mao & Di Stefano 1995; Gaudi & Gould 1997a; Dominik 1998).

2.2. *Lensing Planetary Systems*

A special case of a multiple lens is a star with a planetary system. For certain geometries, a planet separated from its primary by an angular distance comparable to θ_E of the primary lens can create dramatic sharp peaks in the light curve, with durations of a few hours to a few days (Mao & Paczyński 1991), as long as the caustic structure does not resolve the source too severely. Photometry sensitive to 4%–5% deviations would result in detection efficiencies of $\gtrsim$15%–20% for Jupiter-mass planets in the "lensing zone," i.e., Jupiters with projected angular separations (in units of the Einstein ring radius) of $0.6 \lesssim b \lesssim 1.6$ (Gould & Loeb 1992; Bolatto & Falco 1994). Well-monitored events of very high magnification ($A \gtrsim 10$, corresponding to $u_{\min} \lesssim 0.1$) have detection sensitivities to anomalies caused by planets anywhere in the lensing zone that approach 100% (Griest & Safizadeh 1998); such events are also more likely to betray the presence of multiple planets (Gaudi, Naber, & Sackett 1998). Since a large fraction of Galactic lenses toward the Bulge are believed to be stellar (Paczyński 1994; Zhao, Spergel, & Rich 1995; Han & Gould 1996) with lensing zones between $\sim$1 and $\sim$6 AU, microlensing is ideally suited to searching for planetary systems like our own orbiting stars several kpc distant. If events are monitored densely for a few Einstein times, t_E, planets outside the lensing zone may also be detected via microlensing (Di Stefano & Scalzo 1997).

If extrasolar planetary systems are common, precise microlensing monitoring can produce distributions of planet-lens mass ratios and projected orbital radii. Nondetection of planetary lensing anomalies would place strong constraints on the numbers of Galactic stars with planets of mass greater than that of Neptune orbiting within several AU of their parent. Since the set of light-curve morphologies for lensing planetary systems is large and varied (Mao & Paczyński 1991; Wambsganss 1997), planetary parameters will be degenerate unless densely sampled multiband observations are available (Gaudi & Gould 1997b). The caustic structure of smaller mass planets would resolve most stellar sources, resulting in a severe reduction in the size and chance of a planetary perturbation (Bennett & Rhie 1996). Reliable detection of Earth-mass planets will thus require characterization of 1%–2% deviations against nongiant sources for hundreds of events.

Microlensing is thus a statistical technique for the detection and characterization of planetary systems that is sensitive to a large range in planetary mass, orbital characteristics, and position in the Galaxy. As such, it is complementary to radial velocity, pulsar timing, astrometry, and direct imaging methods that are designed for prolonged and detailed studies of individual objects. Although the field is still young, several reviews of the use of microlensing for the detection of extrasolar planets can be found in the literature (Paczyński 1996; Peale 1997; Sackett 1997; Sahu 1997).

2.3. *Chromatic Anomalies: Binary Sources, Blends, and Resolved Sources*

Since a gravitational field deflects light of all wavelengths identically, one of the most fundamental characteristics of microlensing is the achromaticity of the resulting light curve. Nevertheless, color variations, or chromaticity, can occur if the light is generated by anything other than a simple point source. Binary (unresolved) source stars can create anomalies in light-curve shape and chromaticity as first one and then the other of the pair is lensed (Griest & Hu 1992; Han & Gould 1997). A blend of a single source star with unassociated foreground star(s) can also create an anomaly (Di Stefano & Esin 1995), which can be easily described by modifying equation (2) to include an additional term B to account for the sum of all flux from *unlensed* stars that might lie at small enough projected distances that they are unresolved. Since these stars will in general have a different color from the lensed source, the peak of the microlensing light curve will have a color closer to that of the lensed star, returning to the color of the average combined flux at baseline. Blends are important to characterize, since errors in estimates of the event timescales and survey sensitivities will otherwise occur (Di Stefano & Esin 1995; Alard 1997; Wozniak & Paczyński 1997; Han 1997). Any light emitted by the lens itself will also cause blending (Nemiroff 1997), and since a large fraction of Galactic lenses may be stellar (Paczyński 1994; Sahu 1994; Zhao et al. 1995; Han & Gould 1996), this may occur with some frequency. It has been suggested that measuring the frequency and strength of blending as a function of event duration could be used to obtain constraints on the mass of stellar lenses (Buchalter, Kamionkowski, & Rich 1996).

If the source has an angular size that is large compared to that over which the magnification pattern varies, finite size (or extended source) effects will cause the subsequent light curve to deviate from the form given in equations (2)–(4). In particular, the peak of the light curve will be somewhat flattened (Witt & Mao 1994; Peng 1997), an effect that has been reported in one case (Alcock et al. 1997b). Whenever a point lens or any part of a caustic curve transits the source face, the lensing structure acts as a large-aperture, high-resolution telescope, selectively magnifying some parts of the source much more than others. Since the resulting light curve becomes broadened by an amount that depends on the size of the star (which can generally be determined through spectral typing) and on the transverse speed $v_\perp$, high-precision measurements of transit events can determine the relative proper motion of the lens, thus partially breaking the degeneracy otherwise present in equation (4). Furthermore, since stars are limb-darkened by an amount that is wavelength dependent, color variations of a few percent can also be expected during transit events, and precise measurements of the resulting photometric and spectroscopic anomalies can lead to powerful constraints on stellar atmosphere models (Loeb & Sasselov 1995; Gould & Welch 1996; Sasselov 1997; Valls-Gabaud 1998).

2.4. *Nonrectilinear Motion: Parallax and Rotating Binaries*

Finally, a deviation from nonrectilinear motion in any one of the components that is significant over the duration of the microlensing signal will create an anomalous light

curve. The orbit of the Earth around the Sun causes a so-called parallax shift in *every* lensing event that, if well characterized, can be used to determine the transverse velocity of the lens-source system in the ecliptic plane. Such parallax events have been reported (Alcock et al. 1995), but reasonable assumptions lead to the conclusion that hourly sampling and $\sim 1\%$ photometry are required to achieve a 10% detection rate (Buchalter & Kamionkowski 1996). The measurement of parallax anomalies would provide crucial information for breaking the standard mass-distance-velocity degeneracy and thus determining the population from which Galactic lenses are drawn. Finally, nonrectilinear motion is expected within a binary source or binary lens system, and depending on the binary geometry, it may be detectable if the event is sufficiently monitored (Han & Gould 1997; Paczyński 1997; Dominik 1998).

3. THE PLANET COLLABORATION

Although a few instances of most of the anomalies described in § 2 have been observed, routine detection has been hampered by lack of continuous, high-precision, high temporal resolution monitoring. PLANET, the Probing Lensing Anomalies NETwork, is a worldwide collaboration of astronomers whose primary goal is to provide this monitoring in order to detect and study microlensing anomalies, with the particular goal of determining the frequency and nature of lensing planetary systems in the Milky Way (Albrow et al. 1996, 1997). PLANET was constituted in early 1995, soon after the first international microlensing meeting in Livermore, at which all the major detection teams pledged their intention to provide public real-time alerts. PLANET uses semidedicated 1 m class telescopes at widely separated longitudes in the southern hemisphere in coordinated monitoring campaigns. The network is capable (in good weather) of providing nearly round-the-clock monitoring of several microlensing events a night; the detection and alert capabilities of the survey teams ensure that these events will be available.

Keying on the electronic alerts provided by the MACHO and OGLE teams, PLANET is able to focus on individual events, thereby achieving higher sampling rates and often higher precision photometry than the detection surveys. In order to optimize their detection sensitivities, survey teams typically photometer several million stars nightly by imaging tens of fields in the Galactic bulge. Their exposure times are adjusted to the median stellar brightness, and sampling times are dictated by the need to monitor as many fields as possible. For the MACHO team, this has typically meant sampling intervals of ~ 24 hr or more for Galactic bulge sources. As discussed in § 4, PLANET photometry is in contrast at least 10 times more frequent. The frequent, precise, multiband photometry of PLANET is especially sensitive to the anomalies described in § 2 that are short-lived compared to the duration of the primary event (source resolution, planetary anomalies, and caustic crossings) and those that can present only small or subtle amplitude variations compared to the standard microlensing curve (planetary anomalies, blending, parallax, and source resolution). In order to obtain stable, precise photometry with the shortest exposure times in all phases of the moon in these dusty bulge fields, the Cousins I band has been chosen as the primary PLANET monitoring band, but additional Johnson V-band monitoring is also performed in order to allow the detection of chromatic anomalies.

PLANET has completed three Galactic bulge observing seasons; results from the 1995 pilot campaign are presented here.

4. THE 1995 PLANET PILOT CAMPAIGN

During the 1995 pilot campaign, PLANET had nearly continuous access for four weeks in June–July to four southern telescopes at three sites: the Dutch 0.91 m and the Bochum 0.6 m telescopes at the European Southern Observatory (ESO) on La Silla, the South African Astronomical Observatory (SAAO) 1.0 m at Sutherland, South Africa, and the Perth Observatory 0.6 m at Bickley in Western Australia. Results from the Dutch 0.91 m, the SAAO 1 m, and the Perth 0.6 m telescopes are presented here; the observational parameters for these telescopes are summarized in Table 1. Beginning with the 1996 season, the Canopus 1 m telescope near Hobart, Tasmania joined PLANET, greatly improving the longitude coverage of the network.

The large number of real-time microlensing alerts issued by MACHO (Pratt et al. 1996) and OGLE (Udalski et al. 1994a) ensured that PLANET telescopes were continuously observing ongoing microlensing events whenever the bulge was visible (see Fig. 1). Dense monitoring can be performed only after an alert; the postalert portions of the 1995 curves falling within the 1995 PLANET season are shown as solid lines in Figure 1.

In total, PLANET monitored 11 events toward the Galactic bulge in 1995, ten during the primary campaign in June and July, and one during scattered observations in September, when a few baseline points were obtained for earlier events. Light curves for ten of these 11 events are presented here; since only a few data points were collected for MACHO 95–BLG-25, it has been excluded from this analysis.

Mountaintop reduction proceeded in near real-time using DAOPHOT (Stetson 1987) at La Silla and Perth, and DoPHOT (Schechter, Mateo, & Saha 1993) at SAAO. All sites performed their own reduction and communicated with one another almost daily so that the observing strategy

TABLE 1

OBSERVATIONAL PARAMETERS FOR THE PLANET 1995 PILOT OBSERVING SEASON

Telescope	Longitude (deg)	Latitude (deg)	Pixel Scale (arcsec)	CCD Format	Dates of Observation	Seeing[a] (arcsec)
Dutch 0.91 m.....	289.27	−29.25	0.44	512 × 512	Jun 12–Jul 13[b]	1.40
SAAO 1.0 m.....	20.81	−32.38	0.35	512 × 512	Jun 20–Jul 17	1.65
Perth 0.6 m.....	116.13	−32.01	0.58	576 × 384	Jun 15–Jul 16	2.30

[a] Median seeing for observations reported here.
[b] Scattered additional observations were also performed in September and October.

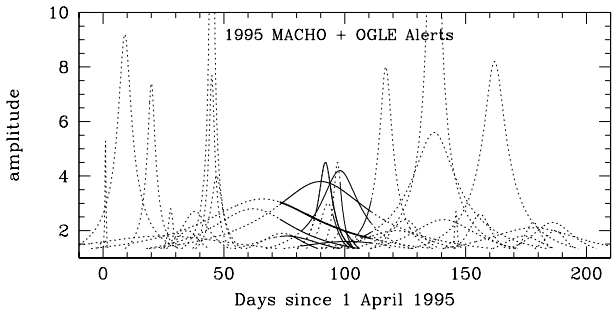

FIG. 1.—Light curves (total magnification as a function of time) are shown for the 1995 real-time electronic alerts given by the MACHO and OGLE microlensing detection teams. Parameters for the light curves are taken from the MACHO alert web page. The 1995 PLANET pilot season corresponds to days 73 to 111 on this plot, during which time the majority of ongoing events were monitored.

could be revised as necessary. In order to track the progress of the events in all weather conditions and to facilitate intersite communication, ten stars were chosen in each field as secondary standards. The flux of the microlensed source was expressed as a fraction of the average flux of these reference stars, which was calibrated later against photometric standards. The behavior of the reference stars also served as an indicator of reduction difficulties with a particular image due to poor seeing, guiding errors, or transparency fluctuations.

Individual light curves were sampled every 1–2 hr; monitoring proceeded primarily in the I band, with occasional V observations interleaved. Exposure times were varied according to the conditions, phase of the moon, waveband, and event magnitude, but were typically 5 minutes in I and about twice as long in V. A summary of the observations from each site is presented in Table 2. In Figure 2, a histogram of the interval between successive PLANET observations of a given event, summed over all events monitored in 1995, is shown for both of the primary observational bands, indicating that a median sampling time for each event of about once per 2 hr in the I band and once per 7 hr in the V band was realized over the duration of the campaign. Although the primary peak in the histogram of Figure 2 illustrates that the longitude coverage of PLANET telescopes is such that $\sim$2 hr sampling was generally possible, the broad secondary peak near 18 hr is an indication

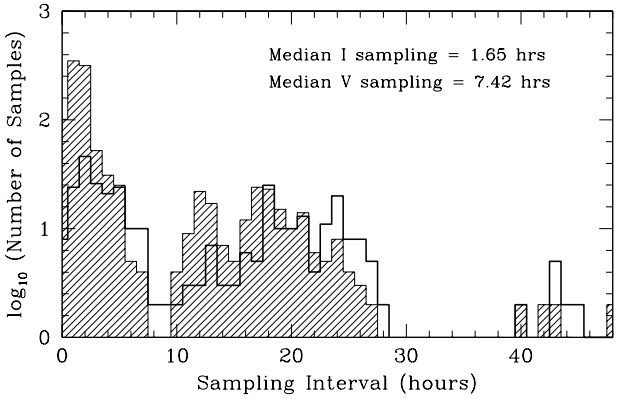

FIG. 2.—Histogram on a logarithmic scale showing the time between PLANET photometric measurements (per event) in 1995, all three stations combined. The shaded histogram shows the I-band sampling, which has a median value of about 1.65 hr; the open histogram with a darker border shows the V-band sampling, with a median of about 7.42 hr.

TABLE 2

NUMBER OF REDUCED FRAMES

	La Silla 0.9 m		SAAO 1.0 m		Perth 0.6 m	
Event[a]	I	V	I	V	I	Total
MACHO 95–BLG-10.....	109	37	48	14		208
MACHO 95–BLG-12.....	122	32	78	38	26	296
MACHO 95–BLG-13.....	152	41	78	59	21	351
MACHO 95–BLG-17.....	93	24	10			127
MACHO 95–BLG-18.....	65	13	23	6		107
MACHO 95–BLG-19.....	72	21	56	18		167
MACHO 95–BLG-21.....			11			11
MACHO 95–BLG-24.....	13	6	9	5		33
MACHO 95–BLG-30.....	29	25				54
OGLE 95–BLG-04.....	78	28	23	7		136

[a] The name of the event, as designated by the discovery team, is given in the first column.

that primarily poor weather, and to a lesser extent scheduling constraints (Table 1), occasionally limited sampling to one or two sites only.

A description of the final data reduction with DoPHOT and a discussion of the resulting photometric precision achieved in these crowded fields are presented in §§ 5 and 6.

5. DATA REDUCTION

Since the primary aim of the campaign was to respond to anomalies in the light curves and to measure them precisely, it was important to be able to carry out photometry at the telescope. As soon as images were obtained, they were debiased and flat-fielded with mean flats previously obtained at twilight, in preparation for measurement. At La Silla and Perth, the DAOPHOT (Stetson 1987) package was used to photometer the frames, while DoPHOT (Schechter et al. 1993) was preferred at SAAO. This difference of approach reflected the exploratory nature of our first observing campaign; each site had experience with a particular program, and it was not obvious at the outset which would be more suitable. In the end, DAOPHOT proved too slow to allow real-time reductions to be performed.

Ten comparison stars near the lens were chosen by the La Silla observer from the first frame obtained for a given event. By referring the measured brightness of the lensed object to the mean brightness of these relatively bright, uncrowded stars, the observer produced over the course of the run a light curve that was independent of observing conditions. In addition, relative photometry from the different sites could be combined easily. This approach proved to be highly successful, and resulted in the discovery of the binary nature of MACHO 95–BLG-12 by PLANET while observations were in progress.

Since the many other stars on each frame apart from the lensed object can be used for variable star and Galactic structure studies, it was decided to reduce all the frames again in a more consistent manner. The crowded-field photometry package DoPHOT (Version 2) was used for this final data reduction. To improve photometric precision, a catalog of positions was used for objects in each microlens field. This catalog was derived from a full reduction of the best-quality image for the field. All other images were first partially reduced to give positions for the brighter stars; these positions were then used to derive geometric trans-

formations with respect to the reference image. On any given image, objects were measured only at the transformed catalog positions. This reduces the number of DoPHOT fitting parameters from 7 to 5 for the brighter (PSF) stars and to 2 for the fainter ones.

To set the relative magnitude zero point, the ten reference stars per field chosen during the observing run were used. Of these, only the ones that were relatively uncrowded (i.e., DoPHOT type = 1 in all but the very worst observing conditions) and stable were selected for the final reduction. These criteria eliminated 12 of the 100 original mountaintop reference stars; two were clearly variable and four others possibly so, while the remainder were judged to be too crowded.

5.1. *Combination of Data*

Discussion of the photometric behavior of a given lens is best done in terms of the differential photometry described above, for which the data precision is highest. The different filters and detectors employed at each observing site could present potential problems when combining data from all sites. Differences between the effective wavelengths of the particular filter/detector combinations used at two sites would lead to a color-dependent difference between their light curves for a given object. Comparison of the SAAO and La Silla data for the reference stars in all our fields shows that they are related by

$$v_L = v_S - 0.086(v - i)_S + C_v$$
$$i_L = i_S - 0.005(v - i)_S + C_i ,$$

where subscripts denote magnitudes in the natural systems as observed at La Silla (L) and SAAO (S), and C_v and C_i are constants. These equations imply that while the i filters at the two sites had similar passbands, the v filter at La Silla had a somewhat redder effective wavelength that the one at SAAO. Since the lens magnitudes were obtained differentially with respect to the mean magnitude of the reference stars, when combining data we have

$$v_{L,\mathrm{lens}} - \langle v\rangle_{L,\mathrm{ref}} = v_{S,\mathrm{lens}} - \langle v\rangle_{S,\mathrm{ref}} - 0.086[(v - i)_{S,\mathrm{lens}} - \langle v - i\rangle_{S,\mathrm{ref}}] ,$$

where $\langle\rangle$ denotes the mean magnitude or color. A similar expression, with a coefficient 0.005, is obtained for i. Thus, there should be little effect from differences in filters and detectors for the i-magnitudes, and, provided that the mean color of the reference stars is sufficiently close to that of the lensed object, only a small effect for the v magnitudes.

The discussion above concerns the relation between La Silla and SAAO photometry only. Sufficient data is not available to study the relationship between photometry at these sites and at Perth. Perth contributed data for two microlensing events, for each of which a simple offset was sufficient to align the light curves photometrically. The i-band filters of all three sites are thus probably quite similar.

5.2. *Transformation to Standard System*

To compare our data with those produced by other groups, it is necessary to convert all data to a common, standard system, which requires transformation equations and an inevitable loss of precision. Standardization is also necessary for astrophysical studies based on stars other than the lens in our observed fields; for example, the distribution of reddening, metallicity, and stellar populations. Almost all of the standard star observations during the 1995 pilot campaign came from La Silla, but since absolute photometric calibration had lower priority than monitoring many lenses with the highest possible time resolution, these data were insufficient for determining the color coefficients for the transformation equations for that site.

At La Silla, all of our fields were referred directly to Landolt equatorial standards (Landolt 1983), while at SAAO only one field, namely MACHO 95–BLG-12, was standardized, in this case with respect to E-region standards (Menzies et al. 1989). The transformation equations from the SAAO natural system to the standard system are, however, known from observations made in other contexts to be

$$v_S = V + 0.040(V - I) + Z_{S,V} ,$$
$$i_S = I - 0.043(V - I) + Z_{S,I} .$$

Combining these equations with the ones above for the reference stars implies that the La Silla transformation equations should be

$$v_L = V - 0.053(V - I) + Z_{L,V} ,$$
$$i_L = I - 0.048(V - I) + Z_{L,I} .$$

Since the La Silla data were insufficient to determine the color coefficients, the magnitudes reported in this paper were determined in effect from equations of the form $v_L = V + z_V$ and $i_L = I + z_I$, in which case the zero points would depend on the mean colors of the standard stars, i.e.,

$$z_V = -0.053\langle V - I\rangle_{\mathrm{standards}} + Z_{L,V} = -0.053 + Z_{L,V} ,$$
$$z_I = -0.048\langle V - I\rangle_{\mathrm{standards}} + Z_{L,I} = -0.048 + Z_{L,I} .$$

In practice, the comparison between SAAO and La Silla photometry yields the differences

$$v_S - v_L = 0.051 \pm 0.018(\mathrm{s.d.})$$
$$i_S - i_L = 0.036 \pm 0.020(\mathrm{s.d.}) ,$$

in good agreement with expectations.

The small standard deviations (s.d.) imply that the reference stars in images of this field obtained at the two sites were similarly affected by crowding, in spite of the different focal plane scales. More work is needed to standardize PLANET data properly; the colors recorded in this paper are essentially on the natural system of La Silla in the 1995 season.

6. PHOTOMETRIC ERRORS

Unlike most microlensing detection teams, PLANET does not adjust exposure times to mean conditions and mean field brightness in order to achieve reasonable photometry for the whole field. Instead, in order to obtain the best photometry for the event itself, PLANET photometry is adjusted to the crowding of the event, its current brightness, and the observing conditions on a given night. Consequently, PLANET photometric precision can be superior to that achieved by the detection teams, with relative photometry considerably more certain than the standardized photometry for most identified stars. Since the PLANET reference stars that were used as relative flux standards were chosen to be relatively bright (typically $I_C \sim 15$ or 16) and uncrowded, the error in the relative photometry is domi-

nated by the magnitude and crowding of the target star for all but the very brightest targets.

The fixed-position catalogs of § 5 were produced from the best seeing frame for each field, which typically contained 5000–10,000 stars, about 50%–60% of which could be measured reliably in typical seeing conditions at those sites. The densities of well-measured stars (i.e., DoPHOT types 1, 3, or 7) in these catalogs were thus ~ 0.03 pixel^{-2} or ~ 0.25 FWHM^{-2}, where FWHM is the full-width at half-maximum of the typical seeing disk. In these exceedingly dense conditions, crowding affects photometric precision. Fainter stars, in addition to having smaller signal-to-noise ratios for a given exposure time, are typically also more crowded.

Shown in Figure 3 is the DoPHOT-reported error for the Dutch 0.91 m (at La Silla) field MACHO 95–BLG-12, as a function of the Cousins I-band magnitude (I_C) of the well-measured stars for three different seeing conditions. The exposure time and seeing of the frame displayed in the middle panel were typical for La Silla at 5 minutes and 1.″4, respectively. The top panel displays results for a frame in good seeing (1.″1) and the bottom panel for a frame with quite poor seeing (2.″2). In good seeing, uncertainties can be larger for bright stars, partly because exposure times are typically shorter, and partly because saturation of some pixels can result in a decrease in the signal-to-noise ratio. In the typical conditions, relative photometry with formal errors of $\sim 1\%$, $\sim 2\%$, and $\sim 7\%$ were routinely obtained for $I_C = 15$, 17, and 19, respectively. Poor seeing results in a smaller number of stars for which reliable measurements can be made, even when exposure times are increased. In addition, the reliability of photometry below $I_C \sim 18.5$ deteriorates rapidly in poor seeing. Comparison of the upper and lower panels of Figure 3 indicates that photometry of the faintest stars that can be identified in these dense fields is limited more by crowding than by photon noise—for stars with $I_C \sim 19$, magnitudes measured on the 2.″2 seeing frame are about twice as uncertain as those from the 1.″1 seeing frame, despite the longer exposure for the former.

Although the formal error determined by DoPHOT is meant to reflect the combination of uncertainties introduced by severe blending and photon noise, the actual scatter in a given constant star was generally greater than that reported by DoPHOT. As an indication of the reliability of the formal error, Figure 4 shows the ratio of the actual scatter over all frames for stars of a give I_C to their mean formal DoPHOT error. All stars in the La Silla field of MACHO 95–BLG-12 for which at least 100 measurements were available are included. The ratio is shown separately for those stars with well-behaved PSF (DoPHOT type = 1; *top panel*), ill-defined PSF (type = 7; *middle panel*), and nearby, partially resolved neighbors (type = 3; *bottom panel*). Averaged over all frames, the true scatter appears to be $\lesssim 1.5$ times the mean DoPHOT error. The ratio decreases with increasing magnitude as faint stars in the most crowded conditions (and thus with the largest and most difficult-to-predict scatter) are no longer identified as point sources and fall out of the sample. In the mean, this ratio is not a strong function of DoPHOT type.

Systematic errors were also introduced by the phase and position of the Moon, which especially affected the quality of the V photometry. Nevertheless, useful data were obtained even in full moonlight conditions with the Moon only $\sim 10°$ from the field center, in which case a severe gradient in the background was apparent over the field. High backgrounds from sources other than the Moon, such as scattered light from clouds and reflections in the telescope optics, also caused some deterioration of the final

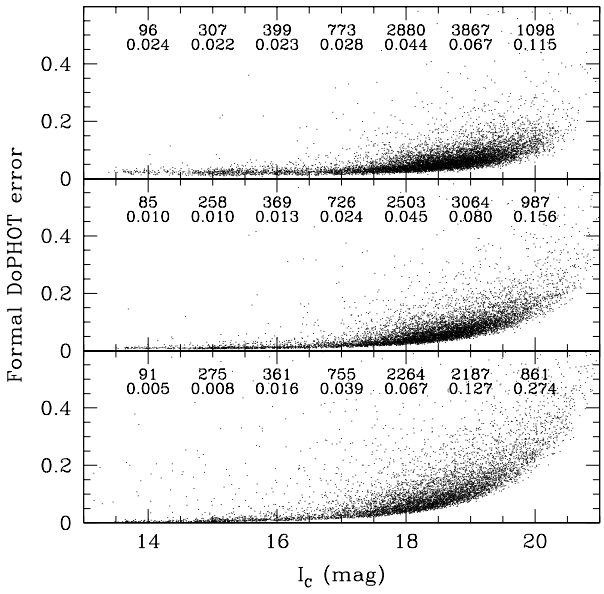

FIG. 3.—Formal DoPHOT error as a function of Cousins I magnitude (I_C) for La Silla observations of the MACHO 95–BLG-12 field in three different seeing conditions of 1.″1 (*top panel*), 1.″4 (*middle panel*), which is typical for this site, and 2.″2 (*bottom panel*), representative of the worst seeing in which data was taken at La Silla. The number of stars and median error (in mag) in each magnitude bin are given above that bin. All measured stellar objects (DoPHOT types = 1, 3, and 7) are plotted.

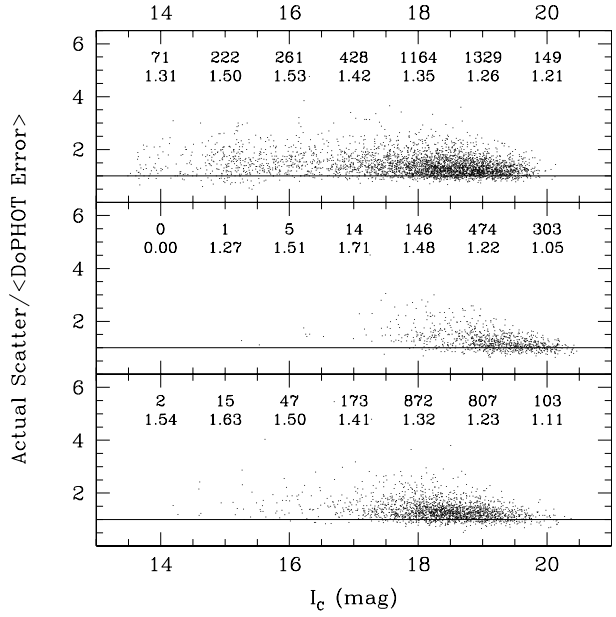

FIG. 4.—Ratio of actual scatter to mean formal DoPHOT error is shown as a function of I_C for the 6587 stars in the La Silla field of MACHO 95–BLG-12 for which at least 100 measurements were available. *Top panel*: Stars with well-behaved PSF (DoPHOT type = 1). *Middle panel*: Stars with ill-determined PSF (type = 7). *Bottom panel*: Stars with nearby, partially resolved neighbors (type = 3). Numbers at the top of each panel indicate the number of stars and median ratio in each magnitude bin.

photometry, although this was seldom severe. Small systematic effects correlated with image quality were also observed.

Many systematic effects could be detected by examining the night-to-night behavior of constant stars, in particular the reference stars, in the same field. This technique was found to be so valuable for rejecting spurious systematic photometric deviations that PLANET online reduction automatically produces graphics such as that displayed in Figure 5 to aid real-time analysis. The apparently discrepant points in the event light curve near dates 174 and 185 seen in Figure 5, and the possible systematic effects seen near the beginning of this segment of the light curve, coincide with poor seeing and are also apparent in the photometry of some of the reference stars. Such systematic effects indicate the necessity of examining the light curves of constant stars in addition to that of the event (with associated computed error bars) when exploring the possibility that a microlensing anomaly has been detected.

7. THE RESULTS

The rapid, precise, and continuous multiband monitoring required for our primary program is also suited to the discovery and study of many types of Galactic variable stars. Searches for periodic light curves typically produce several variable stars per PLANET field, some with rather extreme or difficult-to-observe characteristics, including periods of only a few hours, amplitudes under 5%, or minima of $I \sim 19$. The variable-star studies will be presented elsewhere; here we focus on the results of our microlensing monitoring.

The ten microlensing events closely monitored by PLANET in 1995 and their immediate stellar environs are shown in the gray-scale I-band images of Figure 6. All frames were taken at the Dutch 0.91 m at ESO, with the exception of MACHO 95–BLG-21, which was taken at the SAAO 1 m. The contrast has been logarithmically adjusted to illustrate the crowding conditions of each source star. Since the events were already in progress at the time of these PLANET observations, the microlensed star appears brighter (relative to its neighbors) than it would in a baseline finding chart.

Three of the ten events (MACHO 95–BLG-10, 95–BLG-17, and OGLE 95–BLG-04) were so severely crowded as to appear to be optical doubles (DoPHOT type 3); in all seeing conditions, their point spread function (PSF) was too

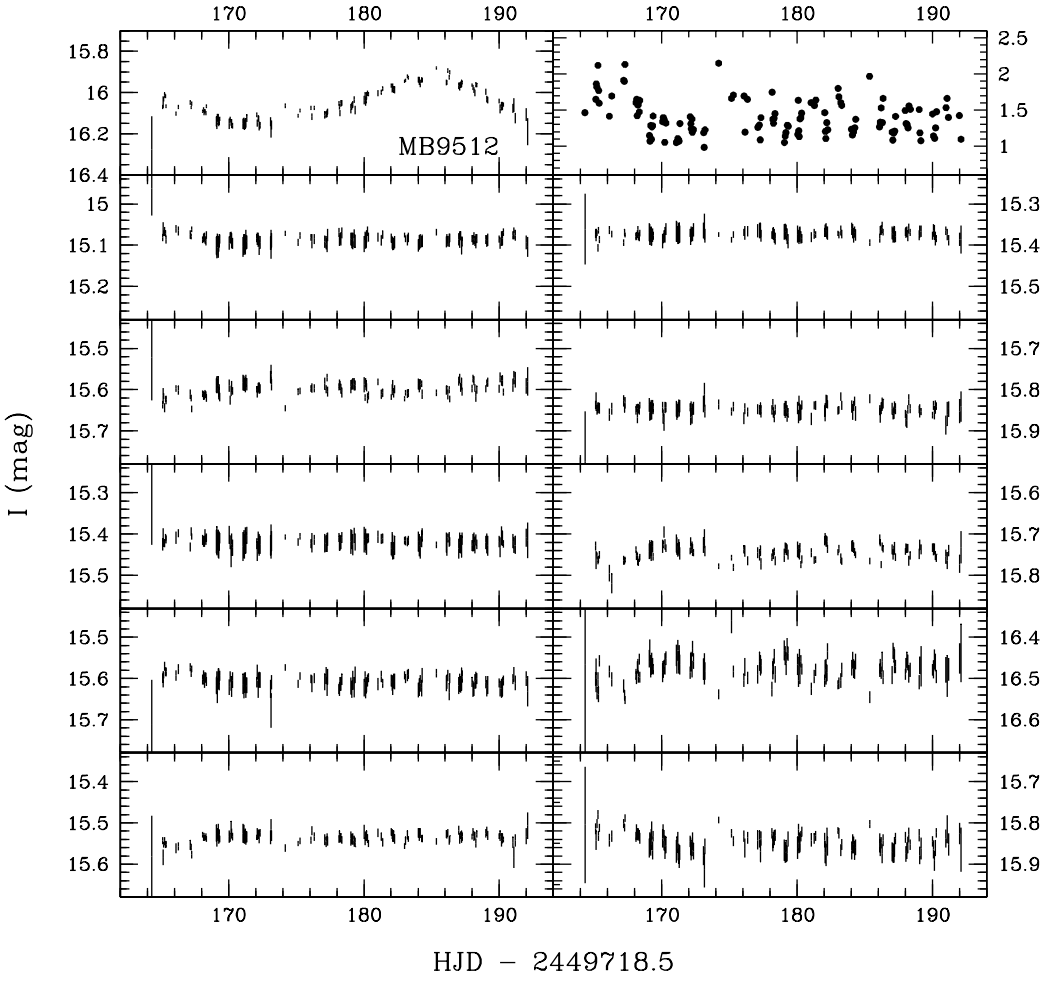

FIG. 5.—La Silla I-band light curve for the binary event MACHO 95–BLG-12 (MB9512) is shown in the upper left-hand panel, together with the seeing for each frame in the upper right-hand panel, and the light curves of the ten reference stars in the lower panels. Reference stars are displayed on a magnitude scale that is enlarged by a factor of 2 compared to that of the microlensing event. Formal DoPHOT errors are displayed. Note that the apparently discrepant points in the event light curve near dates 174 and 185 coincide with poor seeing, and are also discrepant in the photometry of some of the reference stars.

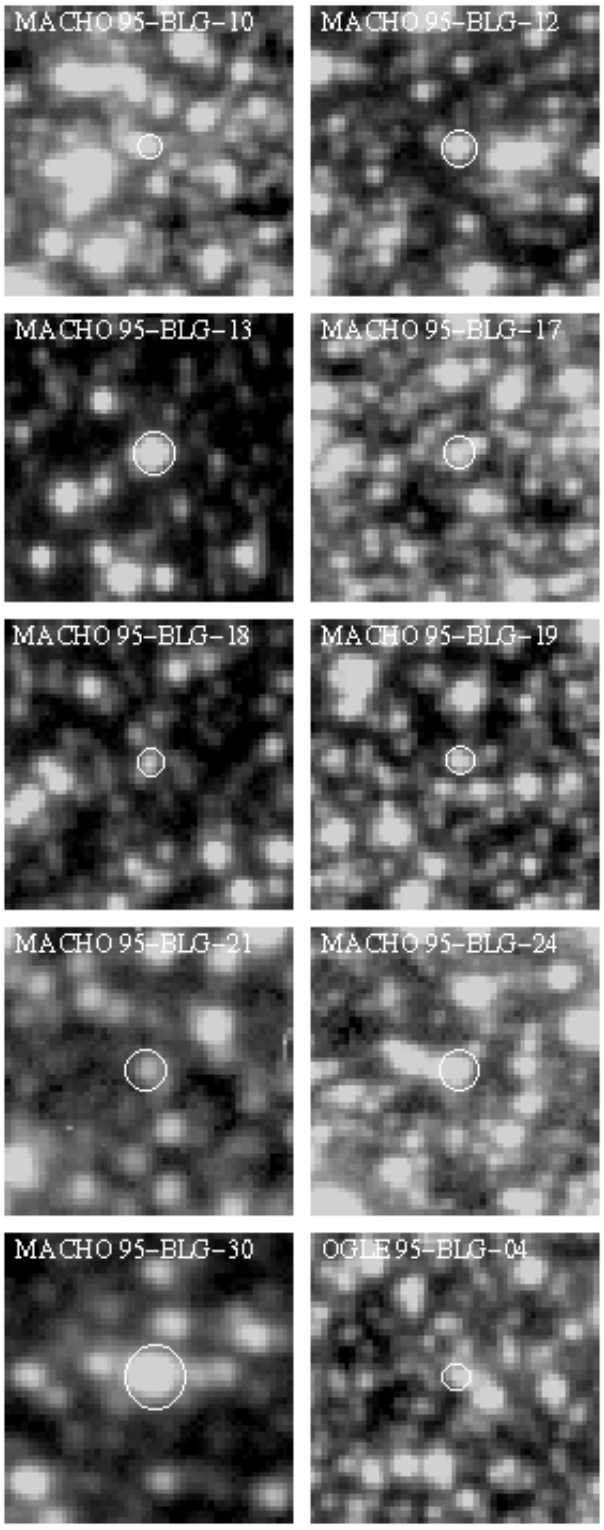

FIG. 6.—PLANET finding charts for the microlensing fields monitored closely in the 1995 campaign; the source star is indicated with an open circle. The logarithmic contrast has been chosen to emphasize faint stars in the field and to illustrate the crowding conditions for each event. The MACHO 95–BLG-21 field is 23″ on a side and was taken in 1.″3 seeing. All other images are 18″ on a side and have seeing of 1.″0–1.″1. North is up and east to the right.

strongly blended with a neighbor to allow an independent photometric solution. Figure 6 illustrates this crowding visually, and light curves shown in Figures 7 and 8 demonstrate that this is translated into larger photometric scatter

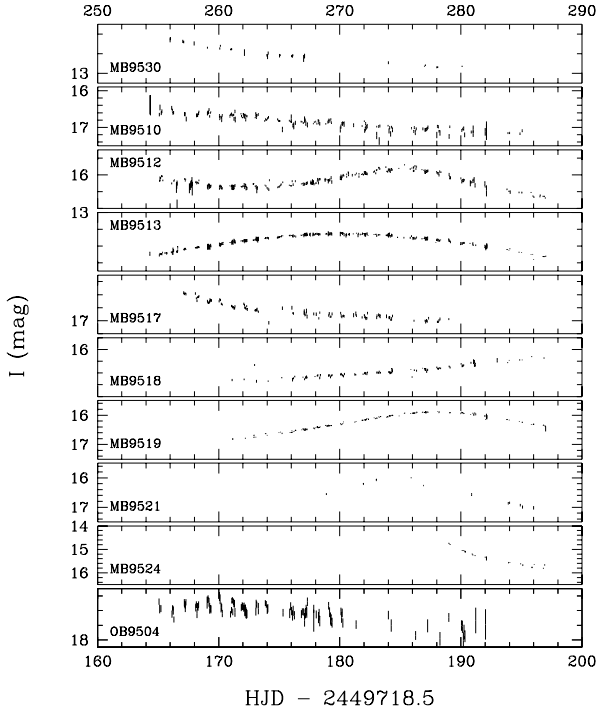

FIG. 7.—Combined *I*-band light curves from all PLANET sites of the nine closely monitored events in the 1995 pilot season, and one extra event (MACHO 95–BLG-30) monitored by PLANET in additional observations later that year. The length of the error bar represents the formal DoPHOT error. All points are shown with no averaging or binning, so that the scatter gives a correct indication of the true uncertainty in the relative photometry. For every plot, a small tick mark on the vertical axis represents 0.2 mag. Abbreviated names for the events (e.g., MB9530 = MACHO 95–BLG-30) are used to enhance legibility.

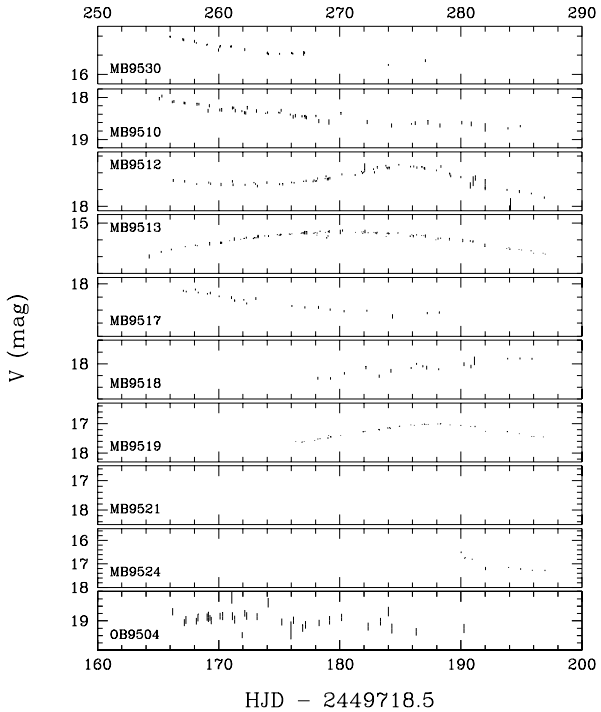

FIG. 8.—Same as Fig. 5, but for the *V* band. Data from all sites are shown. For every plot, a small tick mark on the vertical axis represents 0.2 mag. No *V*-band data were obtained for MACHO 95–BLG-21.

TABLE 3

PLANET-DERIVED EVENT PARAMETERS

Event	I[a]	$V-I$[b]	A_{max}	t_0[c]	t_E (days)
MACHO 95–BLG-10.....	17.5 (0.3)	1.59 (0.11)	3.3 (0.6)	151[d]	49 (24)
MACHO 95–BLG-12.....	17.03 (0.14)	1.63 (0.04)	...	...	...
MACHO 95–BLG-13.....	14.75 (0.04)	1.85 (0.03)	3.95 (0.12)	180.3 (0.5)	76.2 (5.0)
MACHO 95–BLG-17.....	17.00 (0.04)	1.48 (0.04)	1.61 (0.16)	163[d]	8.9 (1.5)
MACHO 95–BLG-18.....	17.16 (0.08)	1.75 (0.07)	2.5 (0.2)	204 (6)	61.5 (7.0)
MACHO 95–BLG-19.....	17.62 (0.32)	1.12 (0.04)	4.93 (1.4)	187.9 (0.21)	35.4 (12.3)
MACHO 95–BLG-21.....	...	...	2.83 (0.28)	184.5 (0.16)	7.4 (2.40)
MACHO 95–BLG-24.....	15.8 (0.08)	1.64 (0.06)	...	186[d]	...
MACHO 95–BLG-30.....	13.08 (0.08)	2.97 (0.02)	25[d]	226[d]	35.7 (4.7)
OGLE 95–BLG-04.....	17.9 (0.37)	1.40 (0.13)	1.36 (0.45)	170.9 (4.8)	11 (15)

NOTE.—Colors and magnitudes have not been dereddened; quoted uncertainties do not include an approximate 14% uncertainty from transformation to the standard system.

[a] Baseline Cousins I magnitudes are determined from fits.

[b] $V-I$ color is determined from a common fit to data unless otherwise noted.

[c] HJD 2449718.5.

[d] Held fixed at the MACHO-determined value.

than for unblended events (DoPHOT type 1) of comparable brightness.

7.1. *The Microlensing Light Curves*

The light curve of each monitored event is shown in Figures 7 and 8, in the I and V bands, respectively.[7] All data from all sites are shown, except those for which the image quality was so poor that the event could not be associated with an identifiable stellar PSF, or for which one or more of the final reference stars was so severely blended so as to appear double. The event flux has been normalized in each frame by the average flux for the final reference stars chosen for that field. Calibration of the reference stars during photometric conditions then sets the absolute scale. Error bars reflecting the formal error returned by DoPHOT accompany each point in Figures 7 and 8, and are often no larger than the size of the plotted point. MACHO 95–BLG-30 was monitored outside the regular pilot season from La Silla only, and thus has a different timescale, which is shown at the top of each figure.

7.2. *Fitted Event Parameters*

Relative photometry of stars in the monitored fields differed by up to a few percent among PLANET sites, even though the same set of reference stars was used. The offsets differed for different stars in the same field; no trend was discovered between the mean size or sense of the offset for a star and its stellar magnitude or color. Fainter stars exhibited larger scatter in their offsets, which may be because they are more likely to be severely crowded. Different detector resolutions and seeing conditions at each site, coupled with the severe crowding in all of the fields, may be responsible for these small site-dependent differences in relative photometry.

The size of the scatter in the offsets within a given field prevented the assignment of a fixed offset per field or per site. To determine the size of the offset for a given microlensing event, we further cleaned the light curve by removing all images in which the seeing was above 1.″85 or in which the reference stars showed scatter much larger than the formal DoPHOT errors, which is an indication of unsatisfactory photometric reduction. This supercleaning procedure generally removed no more than 5%–10% of all reduced frames in each field. We then performed a combined fit to the supercleaned data from all sites within a given waveband with point-lens, point-source microlensing light curves (eq. [3]), allowing the site-to-site offsets (assumed to be multiplicative in flux) to float as free parameters for each band. (For MACHO 95–BLG-12, which shows clear indications of its binarity, the offset was determined by eye.) The incompleteness of our light curves caused by the finite length of our pilot campaign or post-peak alerts by the detection teams often resulted in ill-constrained fits to the standard point-lens, point-source form, especially where data were missing at peak magnification or at the baseline. Although a unique determination for all the standard microlensing parameters, A_{max}, t_0, t_E, and F_0, was generally not possible, the fitting procedure always produced robust, well-determined offsets, typically on the order of a few percent, even when different constraints were placed on the other lensing parameters. These offsets were used to photometrically align the multisite light-curve data shown in Figures 7 and 8.

Although we were able to gather a few baseline points for most of our light curves in scattered observations after our pilot campaign, the relative baseline flux in the I and V bands from these observations is generally only known to within $\sim$10%. The $V-I$ color of the source star in our own system of filters and reference stars can be determined quite accurately using the method described above to determine offsets between multisite data, but transformation of the color to the standard system introduces an additional uncertainty of about $\sim$14%. Baseline magnitudes and colors for the events were determined by simultaneously fitting all supercleaned I and V data, and are reported in Table 3. The magnitudes and colors are not dereddened. Fitting uncertainties are indicated in parentheses. Errors associated with transformation to the standard system have not been included, since a more careful calibration of our fields is planned that will significantly reduce these uncertainties. Only reasonably constrained event parameters are listed in Table 3; in a few cases where our coverage was particularly insufficient, parameters that were poorly determined by PLANET photometry were held fixed at their

[7] All light curve data reported here, including those for the reference stars used in each field, can be found at the PLANET web site: http://www.astro.rug.nl/$\sim$planet.

MACHO-derived values in order to better constrain the remaining parameters.

Residuals about these combined fits are shown in Figure 9, where I (*open circles*) and V (*filled circles*) residuals are shown on the same scale for each event. The 1 σ scatter in the residuals ranged as small as 0.87% for the I data of MACHO 95–BLG-13, to as large as 15% for the V data of the faint event OGLE 95–BLG-04, but were typically 4% $\pm$ 3% for the I data and 5% $\pm$ 4% for the V data. Note that this is consistent with expectations for the uncertainty in our relative photometry based on constant stars.

The robustness of the fitted parameters for well-sampled events is shown in Figure 10, which displays separate fits to the PLANET I- and V-band light curves of MACHO 95–BLG-13 superposed on the data. No binning has been performed, so that the true scatter could be appreciated. Error bars are formal DoPHOT uncertainties. An inset enlarges the region at peak magnification, and arrows indicate the positions of scattered baseline points obtained after the official pilot season, whose small error bars on this curve might otherwise go unnoticed. The presence of these points near the baseline significantly reduced the fit uncertainties. Within these uncertainties, all event parameters are identical for the separate V- and I-band fits.

Comparison of Tables 3 and 4 indicates that the baseline magnitudes derived by PLANET and those derived by the detection teams agree within the uncertainties (including those from our transformation to a standard photometric system and the $\sim$10% uncertainty in MACHO absolute photometry). In addition, where we were able to perform relative photometry on MACHO (baseline) finding charts,

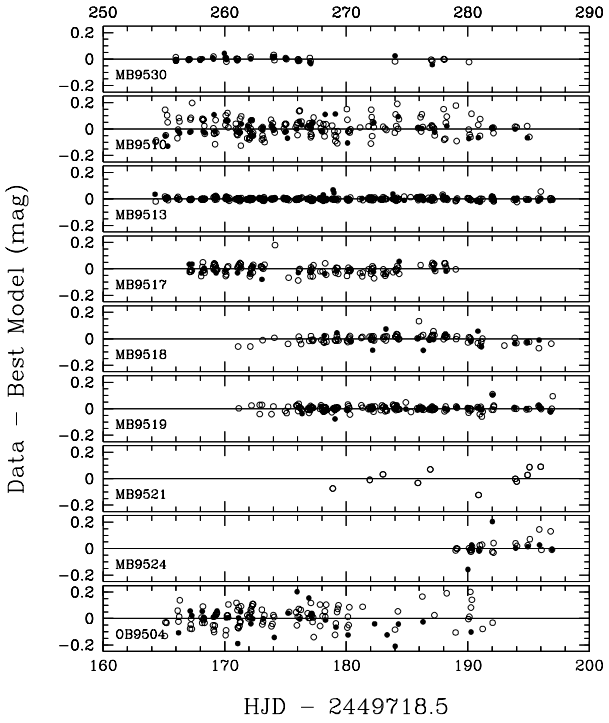

FIG. 9.—I-band (*open circles*) and V-band (*filled circles*) residuals from the best point-lens point-source fits to all data are plotted separately to the scale for each event. All cleaned data are shown individually. The scatter in the residuals for MACHO 95–BLG-13 and 95–BLG-19 is smaller than the size of the points, so that the hundreds of open circles indicating the I data are almost completely obliterated by the filled circles of the V data. The most crowded events clearly show the most scatter.

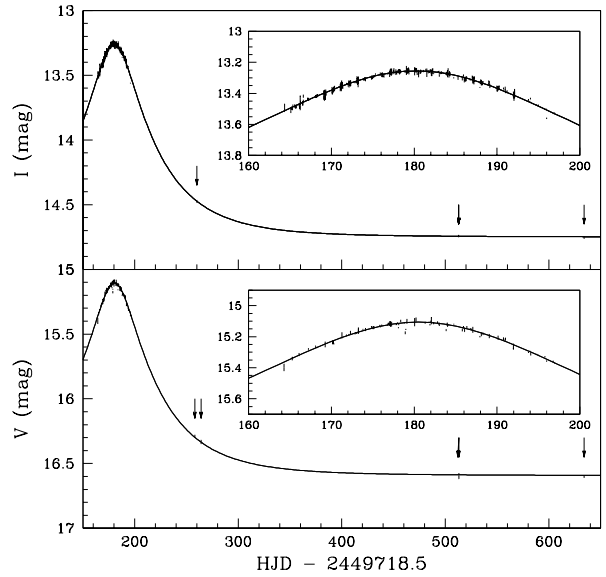

FIG. 10.—Separate fits to the PLANET I- and V-band data are shown for event MACHO 95–BLG-13. All data are shown (without binning) with their associated formal DoPHOT error bars. Scattered baseline points are indicated with arrows. Within the uncertainties, all event parameters are identical for the separate V- and I-band fits.

these also agreed with our fitted baselines to within the estimated uncertainties associated with transforming from MACHO R to I_C.

Without uncertainties for the values of A_{max}, t_0, and t_E derived by the detection teams, it is difficult to assess the relationship between our fitted parameters and theirs, although there do appear to be a few real discrepancies. In particular, the PLANET light curve for MACHO 95–BLG-18 in Figures 7 and 8 is clearly rising beyond the MACHO-reported peak. This may be related to the larger timescale and larger amplitude reported by PLANET for these events, if the MACHO estimates were not based on post-peak data. In addition, the event may be more blended in MACHO photometry than in PLANET images, resulting in decreased MACHO estimates for the timescale and amplitude. For two other events, MACHO 95–BLG-17 and 95–BLG-21, PLANET reports apparently shorter timescales than does MACHO. For this we have no explanation, but do note that we have three baseline points for MACHO 95–BLG-17, but none for 95–BLG-21. The longer observing runs realized by PLANET in 1996 and 1997 and the additional baseline photometry taken for events monitored in those seasons are expected to lead to microlensing parameters that are considerably better constrained for 1996 and 1997 events.

Given the precision and density of the photometry obtained over finite portions of ten light curves monitored by PLANET in its 1995 pilot season, the remainder of this section will be devoted to the two types of anomalies to which this data set is most sensitive: chromaticity and binary lenses with moderate mass ratios, such as those produced by binary star systems or massive extrasolar planets.

7.3. *Chromaticity*

In order to test for chromaticity in the light curves, we have binned the I and V data in 24 hr periods and then computed the $V-I$ color deviation in this period relative to the mean color of the event. The results are shown in Figure

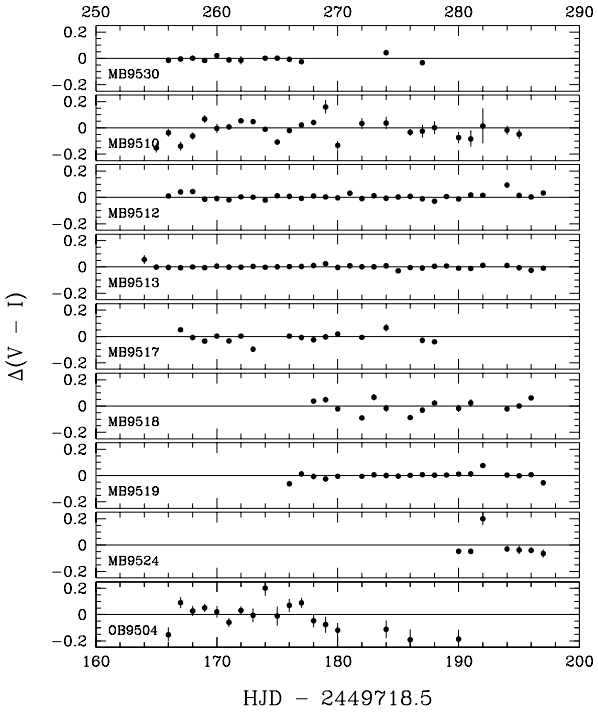

FIG. 11.—All cleaned I- and V-band data have been binned into 24 hr segments and then subtracted to produce color deviations in magnitudes vs. time. The mean color of the event is used as the reference color. No V-band data are available for MACHO 95–BLG-21. The deviant point for MACHO 95–BLG-24 is due to high sky background in one V frame. OGLE 95–BLG-04 is the faintest and most crowded event in these data; this may cause the color shift with time as the microlensed star decreases in brightness while its companion(s) stays constant.

11. This test could not be performed on MACHO 95–BLG-21, since no V data were available. MACHO 95–BLG-24 shows a large single departure near date 192, apparently redder on this day than on days previous or following. Examination of the light curves shows that the single V-band data point during this 24 hr period was anomalously faint. This appears to be related to the exceedingly high background of that particular V frame, which significantly degraded the photometry of some of the reference stars as well.

The colors residuals of OGLE 95–BLG-04 in Figure 11 show an apparent blueward trend with time, especially after date 178. Considering the ratio of the size of the discrepancy to the formal error in this and other events, the deviation on any given night could easily be spurious. On the other hand, the color trend over the falling portion of the light curve for this, the faintest and most crowded of our events, may be an indication that the chromaticity is real, and caused by blending with a near neighbor. In that case, as the microlensed source decreases in brightness, its (presumably bluer) companion(s) remains constant, resulting in the observed chromaticity. The $V-I$ color reported by OGLE for this event is 1.55, formally consistent with our value of 1.40 ± 0.13, but also with the notion that the PLANET measurement is contaminated by light from blue companions. This may also explain why the residuals are larger for OGLE 95–BLG-04 after date 180 in Figure 9, and why the PLANET-reported I-band baseline (Table 3) is brighter than the OGLE value (Table 4). Furthermore, fixing the baseline at the OGLE-derived estimate never resulted in satisfactory fits. We conclude that OGLE 95–BLG-04 may be blended in some of these PLANET data.

With the exception of the single deviant point in MACHO 95–BLG-24 and the possible trend for OGLE 95–BLG-04, no clear trend of color with time is seen for the other events, with the 1 σ scatters in the color ranging between 1.4% for MACHO 95–BLG-13 to 7.2% for MACHO 95–BLG-10. These are upper limits to the actual chromaticity for these events, since some artificial color deviation is introduced by the binning procedure, which does not account for the difference in the time of night at which the V and I frames were taken for these microlensing events. The I- and V-band residuals to the best-fit models presented in Figure 9 can be used to examine the chromaticity in a model-dependent, but point-by-point basis.

7.4. *Binarity of MACHO 95–BLG-12*

The binary nature of MACHO 95–BLG-12 is quite apparent and was discovered in real-time by PLANET during the course of its observations. Despite the strong departure of the light curve from that expected for a point source lensed by a point lens, this event shows no chromaticity above 2.6%, averaging $V-I$ in 24 hr bins (Fig. 11).

TABLE 4

MACHO- AND OGLE-REPORTED EVENT PARAMETERS

Event	R.A. (J2000)	Decl. (J2000)	V[a]	R[a]	A_{max}	t_0[b]	t_E[c]
MACHO 95–BLG-10.....	17 58 16.0	−29 32 11	18.9	18.0	2.8	151	47.5
MACHO 95–BLG-12.....	18 06 04.8	−29 52 38	18.6	17.7	3.16	155	binary
MACHO 95–BLG-13.....	18 08 47.0	−27 40 47	16.6	15.6	3.8	179	73.5
MACHO 95–BLG-17.....	18 03 01.1	−28 21 09	18.8	18.0	1.9	163	18.5
MACHO 95–BLG-18.....	18 07 20.6	−28 36 51	18.7	17.8	1.6	190	39.5
MACHO 95–BLG-19.....	18 11 32.5	−27 45 27	18.6	17.9	4.2	187	31.5
MACHO 95–BLG-21.....	17 59 42.2	−28 08 42	20.7	19.7	3.0	183	11.0
MACHO 95–BLG-24.....	18 02 54.4	−29 26 30	17.8	16.9	4.5	186	7.0
MACHO 95–BLG-30.....	18 07 04.3	−27 22 06	16.1	14.7	25.0	226	33.9
OGLE 95–BLG-04.....	18 02 07.6	−30 01 13	20.00	18.45[a]	1.8	165	28.0

NOTE.—Taken from OGLE alert notifications and the MACHO alert web page at http://www.darkstar.astro.washington.edu. Units of right ascension are hours, minutes, and seconds, and units of declination are degrees, arcminutes, and arcseconds.

[a] MACHO broadband V and R magnitudes are quoted, except in the case of OGLE 95–BLG-04, for which the V and I magnitudes determined by the OGLE team are given. Uncertainty in MACHO magnitudes are typically ~10%.

[b] Approximate JD 2449718.5, with an uncertainty typically on the order of 1–2 days.

[c] Einstein radius crossing time in days.

Nor does it show the gentle convexity that would be expected at one of the two peaks of a wide binary source event, but is instead more sharply peaked. This evidence is consistent with the hypothesis that MACHO 95–BLG-12 is a binary lens rather than a binary source, but does not constitute a proof. Combination of the densely sampled PLANET data over the second peak and the more sparsely sampled MACHO data over the entire curve (Pratt et al. 1996) would be likely to result in a definitive model.

7.5. *Detection Sensitivity to Massive Extrasolar Planets*

The discovery of the binary nature of MACHO 95–BLG-12 in the PLANET pilot season data makes it clear that PLANET monitoring is sensitive to the detection of binary lenses with components of similar mass. We now discuss the detection sensitivity to binary lenses in which the ratio of the smaller mass, m_p, to that of its primary lens M is quite small; namely, cases in which the partner has planetary mass.

As discussed in § 2, detection sensitivities to lenses with planetary systems have been estimated by a variety of authors who make simplifying assumptions about the nature and numbers of the planetary systems, their distance relative to the source and observer, the region of the light curve monitored, and the precision of the photometry. Computation of the actual detection sensitivity of this PLANET data set (or any other data set) to planetary systems of various types is not trivial, and requires a computation, on a light curve by light curve basis, of the efficiency with which anomalies produced by a planetary binary of given mass ratio and geometry can be detected in the data set. This efficiency will be a function of the sampling rate, the photometric precision, the maximum magnification of the event, the placement and duration of the monitoring period with respect to the time of maximum magnification, the degree of blending, and, for small mass ratios, the size of the source. A full discussion of how these effects can be incorporated into realistic detection sensitivities is beyond the scope of this paper, but will be presented elsewhere (Gaudi & Sackett 1998). The estimate presented below is meant only to place the PLANET pilot season data in proper context by very roughly indicating its sensitivity to planets of given mass ratios; this also serves as an indication of what will be possible in the future.

Not all light curves nor all portions of a given light curve are equally sensitive to the presence of a planet. Furthermore, the region of maximum *detection* will of course depend on the actual (unknown) orbital radii of the planets. Nevertheless, within the Einstein ring ($A > 1.34$) of events of moderate magnification, typical of our data set, light-curve morphology is approximately equally sensitive to anomalies from so-called lensing-zone planets, i.e., those planets with projected separations from their parent star comparable to the primary's Einstein ring radius (Gould & Loeb 1992). The ratio of the planet's mass m_p to that of its primary, $q \equiv m_p/M$, affects both the duration of the anomaly and the frequency with which the anomaly will occur above a certain photometric threshold. The smaller the mass ratio q, the shorter the average duration and the smaller the chance that there will be large photometric deviations in the light curve. The photometric precision of the data will determine the threshold above which anomalies can be detected. As long as the source is not resolved, the average duration scales with $q^{1/2}$, and thus linearly with the Einstein radius crossing time t_E of the primary lens. The photometric sampling interval is thus naturally expressed in units of t_E when discussing the sensitivity to planetary systems of a given mass ratio. If this sampling interval is sufficiently small for a given mass ratio, then the sensitivity to planet detection depends on the total length of light curve (in units of t_E) monitored with a given photometric precision (assuming that all portions of the monitored light curve are equally likely to contain an anomaly).

With these considerations in mind, we wish to combine the light curves for the events monitored by PLANET in the 1995 pilot season into one rough figure-of-merit for planet detection. To do so we have normalized the monitoring period of each light curve by $2(1 - u_{\rm min}^2)^{1/2} t_E$ in order to obtain the fractional length of monitored curve inside the Einstein ring radius ($A > 1.34$). We then sum over all light curves at a given value of the normalized sampling time, $t_S = \Delta t/t_E$. The cumulative normalized light curve length η sampled at normalized intervals less than t_S is shown by the solid curve in Figure 12 as a function of t_S. The dashed curve shows the same cumulative normalized light curve length for those data sets in which the 1 σ scatter from the best-fit model is less than 5% (namely, the PLANET I light curves for MACHO 95–BLG-12, 13, 17, 18, 19, 24, and 30, and the PLANET V light curves for MACHO 95–BLG-12, 13, 19, and 30).

The typical duration of a planetary anomaly is given very roughly by the time required to cross the diameter of the *planetary* Einstein ring, $2t_p = 2(q)^{1/2} t_E$. Assuming a typical t_E of 20 days, and a lensing system half-way between obser-

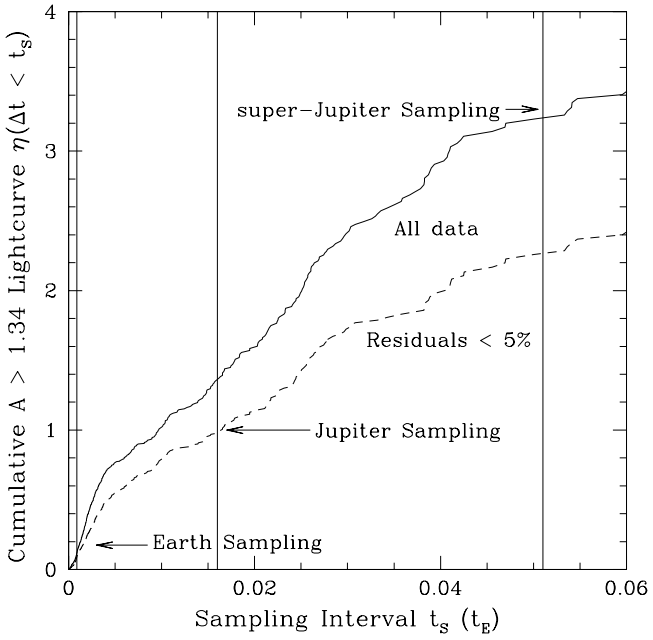

FIG. 12.—Total length of normalized light curve η sampled by PLANET during its pilot season, as a function of the normalized sampling interval t_S (in units of t_E). The full curve shows all data; the dashed curve only shows those data sets that have true scatter of 5% or less from the best-fit models. The vertical lines, which are explained more fully § 7, give approximate minimum sampling intervals appropriate to detecting planets of a given mass ratio q. Light curve data of cumulative length $\eta \gtrsim 6$ must be sampled in order to place constraints on the number of Jupiter-mass planets ($q \sim 0.001$); more massive planets can be constrained more easily, while lower mass planets require more cumulative light curve length.

ver and source, $2t_p \approx 1.7(m_p/M_\oplus)^{1/2}(M/M_\odot)^{-1/2}$ hr $\approx 0.0035(m_p/M_\oplus)^{1/2}(M/M_\odot)^{-1/2}\ t_E$. In order to be able to expect an average of four deviant points over the anomaly, the sampling interval should be no larger than 1/4 of this duration, or $0.0009t_E$, $0.016t_E$, and $0.051t_E$ for Earth-mass, Jupiter-mass, and ten Jupiter–mass (super-Jupiter) planets orbiting solar-type stars, respectively. These maximum sampling intervals are indicated in Figure 12 as vertical lines. Assuming that the primary lens is a solar-type star half-way to the bulge, Figure 12 shows that a total normalized light curve length $\eta \sim 3$ has been monitored with sufficient density to detect super-Jupiters, $\eta \sim 1$ has been monitored often enough to detect Jupiters, and almost none of the total light curve length has been monitored densely enough to detect Earth-mass anomalies.

If all the lenses monitored by PLANET in 1995 have planets with mass ratio $q = 1 \times 10^{-3}$, as would a Jupiter orbiting a solar-mass star, would any have been detected? Gould & Loeb (1992) have shown that, averaged over the portion of the light curve within one Einstein ring radius of the peak, the detection sensitivity to a Jupiter-mass planet at a projected distance of 5 AU from its 1 $M_\odot$ lensing primary is $\sim$17% if the system is located half-way to the Galactic bulge. This sensitivity assumes that deviations of 5% can be reliably detected, in which case a cumulative normalized light curve length of $\eta \sim 6$ must be monitored to produce a single detection, even if all lenses have such planets. Since we have adjusted the maximum sampling interval to expect $\sim$4 deviant points, it is reasonable to assume that the light curves with 5% photometry (Fig. 12, *dashed η curve*) should be sensitive to $\gtrsim$5% deviations at the 2 σ level. Even so, this simple estimate shows that the total length of the $A > 1.34$ light curve monitored in the pilot season was probably insufficient by about a factor of 6 for Jupiter-mass sensitivity.

On the other hand, these pilot-season data may well be sufficient in monitoring frequency, total light curve length, and photometric precision to begin to place limits on the number of super-Jupiters orbiting Galactic lenses. Such systems would have larger detection probabilities and thus require a total light curve length of $\eta \gtrsim 2$ for reasonable detection probabilities (if all lenses have super-Jupiters in their lensing zones). The 1995 pilot-season data, especially in combination with the 1996 and 1997 PLANET data, should be suited to constraining the numbers of such massive extrasolar planets orbiting suns too distant to be seen directly. The existence of such planetary systems can be deduced only with the aid of microlensing monitoring. We stress that the discussion in this section is only intended as an order-of-magnitude estimate; more quantitative results await a full calculation of planetary models and observational efficiencies.

8. CONCLUSIONS AND FUTURE OUTLOOK

The results of the 1995 PLANET pilot campaign conclusively demonstrate the feasibility, challenges, and rewards of microlensing monitoring. PLANET telescopes were continuously and fruitfully employed throughout the month-long campaign, performing photometry with a precision and frequency not feasible for the current microlensing detection programs designed to provide the largest number of alerts.

Despite overhead and weather, monitoring of several events simultaneously proceeded with median sampling times of about 1.6 hr in the I band; V-band monitoring was about 5 times less frequent by design. Real-time mountaintop reduction to track event progress was successfully demonstrated, and by using reference stars in the field as relative flux standards, relative photometry was performed in a wide variety of weather conditions and the data successfully combined between sites on a daily basis. Examination of the photometry of these (constant) reference stars proved crucial in separating systematic effects in the photometry from real anomalous behavior. PLANET relative photometry was able to reach $I = 19$ with an actual precision of 0.10 mag and was ultimately limited more by stellar crowding than by photon noise. The microlensing events showed scatter about their best-fit point-source, point-lens light curves, ranging from $<1\%$ (for PLANET I-band photometry of MACHO 95–BLG-13) to about 15% (for PLANET V-band photometry of OGLE 95–BLG-04), with most residuals at the 4%–5% level.

Two of the ten events showed significant anomalous departures from the point-lens, point-source light curve. The binary nature of MACHO 95–BLG-12 was detected by PLANET in real time on the mountain. Although not conclusive, the shape of the light curve near the second of its two peaks and the lack of $V-I$ chromaticity over the PLANET-monitored portion of the light curve at the 2.5% level suggest that this event is a binary lens rather than a binary source. Definitive modeling will require combining MACHO and PLANET data for this event. OGLE 95–BLG-04, the faintest and most crowded of the events monitored by PLANET, displayed chromaticity at the 20% level over the last half of its PLANET-monitored light curve. This, together with the differences between OGLE and PLANET determinations of the fitted baseline and event duration parameters, suggests that this event may be blended in the PLANET data.

Detailed calculations taking into account the actual sampling times and photometric precision on a light curve by light curve basis will be required before firm estimates can be placed on the planet-detection sensitivity of PLANET observations. Nevertheless, simple considerations indicate that the total length of the microlensing light curve sampled by PLANET in its 1995 pilot season falls somewhat short of placing constraints on the number of lenses with planets of mass 0.001 times that of their primaries (Jupiters), but may be sufficient to constrain the number of planets with mass ratios of 0.01 and higher (super-Jupiters). The detection of Earth-mass planets would require very rapidly sampled (subhourly), high-precision (1%–2%) photometry of hundreds of nongiant stars to generate meaningful constraints.

Looking toward the future, one can use the qualitative and quantitative lessons of the 1995 PLANET pilot campaign to plan more effective observing strategies and to give an indication of what might be expected in the coming years from intense microlensing monitoring.

The number of events that can be monitored per night with telescopes of a given aperture depends on observing overhead, the brightness and crowding of the source star, and the desired level of photometric precision. To achieve the precision realized in the 1995 pilot season, PLANET telescopes monitored about ten events of moderate brightness with better than 2 hr sampling over a period of 1 month. Since the typical duration of an Galactic bulge event (defined as $2t_E$) is on the order of a month, the overall sensitivity to most microlensing anomalies will scale

roughly as the number of months of usable monitoring observations. In subsequent 1996–1998 observing seasons, PLANET has been granted increasingly larger blocs of observing time, making more of the Galactic bulge season accessible. This has resulted in an approximate doubling of the number of events monitored in 1997, and a further increase of a factor of 1.5 is expected in the 1998 season. Longitudinal coverage has been significantly improved with the addition of the Canopus 1 m telescope near Hobart, Tasmania, to the complement of PLANET telescopes; Canopus also serves as a hedge against bad weather at the Perth longitude. Finally, detectors of increased sensitivity have been or are being installed at all PLANET sites. Taken together, these enhancements will serve to increase the sensitivity to planet detection (per bulge season) substantially, compared to the month-long 1995 pilot campaign.

Changes in monitoring strategy may also lead to increased sensitivities to planetary anomalies. In the 1995 pilot season, sampling frequencies were nearly constant at once every 1 to 2 hr, as weather allowed. In subsequent seasons, PLANET has made the conscious decision to scale the interval between adjacent measurements on each light curve with the Einstein crossing time t_E for that event, so as to increase the probability of detecting putative Jupiter-mass planets in the lensing zone of the primary. In this way, the complete data set should have a more uniform detection efficiency in this portion of phase space. Similarly, in order to spend most of the observing resource on the portion of the light curve that is most sensitive to planets in the lensing zone of a few AU, light curves are monitored intensely only while the source is projected within $1–1.5\theta_E$. Eventually, as the number statistics of intensely monitored events increase, it may be sensible to relax these constraints in order to increase sensitivity to planets outside the lensing zone or planetary systems with extreme mass ratios.

Finally, event selection can play an important role in determining the success of achieving particular program goals. In all cases, photometric precision is important, so that whenever possible the choice of (relatively) uncrowded source stars is advisable. Events should be chosen to have timescales t_E short enough to fit comfortably into the observing season, but with postalert durations long enough to allow sufficient sampling at the desired rate. Low impact parameter (high-magnification) events are also favored for planet detection, since the source is always brought near the central caustic, increasing the chance of a detectable anomaly. If the goal is to maximize the detection sensitivity to Earth-mass planets with mass ratios $q \sim 1 \times 10^{-5}$ to 1×10^{-6}, source resolution effects will dilute the amplitude of anomalies if the angular radius of the source star is larger than that of the planetary Einstein ring radius (Bennett & Rhie 1996); this selects against giants or subgiants as source stars. If, on the other hand, the goal is to maximize sensitivity to larger mass ratio planets, giants and subgiants are favored, since their relative brightness will allow more precise photometry with shorter exposures without introducing a bias against lenses of a particular type.

Given the encouraging results of its 1995 pilot campaign, the future of PLANET looks bright as it continues to monitor microlensing events in search of anomalous behavior. Each Galactic bulge season brings an increase in the numbers of electronic alerts being issued by the microlensing survey teams, allowing PLANET to be more selective in choosing events to match its program goals. Together with the increasingly generous awards of telescope time from PLANET-participating sites, this has resulted in an ever-growing database of precise and rapidly monitored microlensing events, increasing the detection sensitivity to anomalies of all kinds, in particular those produced by extrasolar planets in the inner Galaxy.

PLANET thanks the MACHO and OGLE collaborations for providing real-time electronic alerts of microlensing events in progress; copious early alerts are crucial to the success of our intensive microlensing monitoring. In addition, we would like to thank Abi Saha and Mario Mateo for their help in setting up DoPHOT. Financial support from ASTRON, the astronomical division of the Foundation for Nederlands Wetenschapelijk Onderzoek (Dutch Scientific Research), NWO, is gratefully acknowledged. PLANET members also wish to thank the Leids Sterrewacht Foundation, Perth Observatory, and the South African Astronomical Observatory for the generous allocations of time that made this pilot program possible.

REFERENCES

Abe, F., et al. 1997, in Proc. 12th IAP Colloq., Variable Stars and the Astrophysical Returns of Microlensing Surveys, ed. R. Ferlet, J.-P. Maillard, & B. Raban, (Gif-sur-Yvette: Editions Frontières), 75
Alard, C. 1997, A&A, 321, 424
Alard, C., Mao, S., & Guibert, J. 1995, A&A, 300, L17
Alard, C., & Guibert, J. 1997, A&A, 326, 1
Albrow, M., et al. 1996, in Proc. IAU Symp. 173, Astrophysical Applications of Gravitational Lensing, ed. C. Kochanek & J. Hewitt (Dordrecht: Kluwer), 227
———. 1997, in Proc. 12th IAP Colloq., Variable Stars and the Astrophysical Returns of Microlensing Surveys, ed. R. Ferlet, J.-P. Maillard, & B. Raban (Gif-sur-Yvette: Editions Frontières), 135
Alcock, C., et al. 1993, Nature, 365, 621
———. 1995, ApJ, 454, L125
———. 1997a, ApJ, 479, 119
———. 1997b, ApJ, 491, 436
Aubourg, E., et al. 1993, Nature, 365, 623
Bennett, D. P., & Rhie, S. H. 1996, ApJ, 472, 660
Bolatto, A. D., & Falco, E. E. 1994, ApJ, 436, 112
Buchalter, A., & Kamionkowski, M. 1996, ApJ, 482, 782
Buchalter, A., Kamionkowski, M., & Rich, R. M. 1996, ApJ, 469, 676
Crotts, A., & Tomaney, A. B. 1996, ApJ, 473, L87
Di Stefano, R., & Esin, A. A. 1995, ApJ, 448, L1
Di Stefano, R., & Scalzo, R. A. 1998, ApJ, submitted (preprint astro-ph/9711013)
Dominik, M. 1998, A&A, 329, 361
Dominik, M., & Hirshfeld, A. C. 1994, A&A, 289, L31
Einstein, A. 1936, Science, 84, 506
Gaudi, B. S., & Gould, A. 1997a, ApJ, 482, 83
———. 1997b, ApJ, 486, 85
Gaudi, B. S., Naber R. M., & Sackett, P. D. 1998, ApJ, 502, 33
Gaudi, B. S., & Sackett, P. D. 1998, in preparation
Gould, A. 1996, PASP, 108, 465
Gould, A., & Loeb, A. 1992, ApJ, 396, 104
Gould, A., & Welch, D. L. 1996, ApJ, 464, 212
Griest, K., & Hu, W. 1992, ApJ, 397, 62
Griest, K., & Safizadeh, N. 1998, ApJ, 500, 37
Han, C. 1997, ApJ, 490, 51
Han, C., & Gould, A. 1996, ApJ, 467, 540
———. 1997, ApJ, 480, 196
Landolt, A. U. 1983, AJ, 88, 439
Lennon, D., Mao, S., Fuhrman, K., & Gehren, T. 1996, ApJ, 471, L23
Loeb, A., & Sasselov, D. 1995, ApJ, 491, L33
Mao, S., & Di Stefano, R. 1995, ApJ, 440, 22
Mao, S., & Paczyński, B. 1991, ApJ, 374, L37
———. 1996, ApJ, 473, 57
Melchior, A.-L., et al. 1997, A&A, in press (preprint astro-ph/9804321)
Menzies, J. W., Cousins, A. W. J., Banfield, R. M., & Laing, J. D. 1989, SAAO Circ. 13, 1
Nemiroff, R. 1997, ApJ, 486, 693
Paczyński, B. 1986, ApJ, 304, 1
———. 1996, ARA&A, 34, 415
———. 1997, ApJ, submitted (preprint astro-ph/9711007)

Paczyński, B., et al. 1994, ApJ, 435, 113
Peale, S. 1997, Icarus, 127, 269
Peng, E. 1997, ApJ, 475, 43
Pratt, M. R., et al. 1996, in Proc. IAU Symp. 173, Astrophysical Applications of Gravitational Lensing, ed. C. Kochanek & J. Hewitt (Dordrecht: Kluwer), 221
Sackett, P. D. 1997, Final Report of the ESO Working Group on the Detection of Extrasolar Planets, Appendix C (ESO Document: SPG-VLTI-97/002)
Sahu, K. C. 1994, Nature, 370, 275
———. 1997, in ASP Conf. Ser. 119, Planets Beyond the Solar System and the Next Generation of Space Missions, ed. D. Soderblom (San Francisco: ASP), 73
Sasselov, D. D. 1997, in Proc. 12th IAP Colloq., Variable Stars and the Astrophysical Returns of Microlensing Surveys, ed. R. Ferlet, J.-P. Maillard, & B. Raban (Gif-sur-Yvette: Editions Frontières), 141
Schechter, P. L., Mateo, M., & Saha, A. 1993, PASP, 105, 1342
Stetson, P. B. 1987, PASP, 99, 191
Udalski, A., et al. 1993, Acta Astron., 43, 289
———. 1994a, Acta Astron., 44, 227
———. 1994b, ApJ, 436, L103
Valls-Gabaud, D. 1998, MNRAS, 294, 747
Wambsganss, J. 1997, MNRAS, 284, 475
Witt, H., & Mao, S. 1994, ApJ, 430, 505
Wozniak, P., & Paczyński, B. 1997, ApJ, 487, 55
Zhao, H., Spergel, D., & Rich, M. 1995, ApJ, 440, L13